

On the tradeoff between antibiotic efficacy and the selection for resistance in spatial gradients

Matti Gralka[†], Diana Fusco^{†‡}, Stephen Martis[†] and Oskar Hallatschek^{†‡‡}

[†] Department of Physics, University of California, Berkeley, CA 94720

[‡] Biophysics and Evolutionary Dynamics Group, Departments of Physics and Integrative Biology, University of California, Berkeley, CA 94720

Abstract. Since penicillin was discovered about 90 years ago, we have become used to using drugs to eradicate unwanted pathogenic cells. However, using drugs to kill bacteria, viruses or cancer cells has the serious side effect of selecting for mutant types that survive the drug attack. A key question therefore is how one could kill as many cells as possible for a given acceptable risk of drug resistance evolution. We address this general question in a model of drug resistance evolution in spatial drug gradients, which recent experiments and theories have suggested as key drivers of drug resistance. Importantly, our model also includes the influence of convection, resulting for instance from blood flow. Using stochastic simulations, we quantify the trade-off between the killing of wild-type cells and the rise of resistance mutations: shallow gradients and convection into the antibiotic region promote wild-type death, at the cost of increasing the establishment probability of resistance mutations. We can explain these observed trends by modeling the adaptation process as a branching random walk. Our analysis also reveals that the trade-off between death and adaptation depends on a few key control parameters, which compare the strengths of the spatial drug gradient with the convection and random dispersal terms. Our results show in particular that convection can have a momentous effect on the rate of establishment of new mutations, and may heavily impact the efficiency of antibiotic treatment.

1. Introduction

The emergence of drug resistance represents one of the major clinical challenges of the current century [1–3]. Microbial pathogens quickly acquire resistance to new antibiotics [4], while solid tumors often regrow after treatment because of resistance mutations that arise during tumor growth [5]. In addition to genomic studies examining the molecular causes of resistance [6, 7], the dynamics of drug resistance evolution has recently attracted wide interest [8, 9], with the dual goal of understanding the emergence of resistance and developing novel strategies to prevent or control its spread [10, 11]. Next-generation sequencing and high-throughput experimental techniques enable the

[‡] To whom correspondence should be addressed. Email: ohallats@berkeley.edu

quantitative study of resistance evolution but require the development of new theories to appropriately interpret experimental results [12].

In many realistic systems, an evolving population interacts with its surroundings and exhibits a well-defined spatial structure (for instance, in tumors and biofilms [5]). It has recently been shown that this spatial structure can strongly influence the subclonal structure and the adaptation of spatially expanding populations, both from *de novo* and pre-existing mutations [13–15]. Likewise, spatial [12, 16, 17] or temporal [10, 18] gradients in antibiotic concentration can enable populations to reach a higher degree of resistance than in homogeneous drug concentrations, at least in part because they enable the slow accumulation of multiple mutations, each conferring a small amount of resistance.

The presence of spatial drug gradients is well documented both in the outside environment [19, 20] as well as within biofilms [21] and the human body [22–24], and it has been hypothesized that the presence of spatial heterogeneities may facilitate the emergence of drug-resistant phenotypes [25]. In a microfluidic experiment, a spatial gradient indeed gave rise to a higher rate of adaptation of bacterial populations [16]. Similarly, microbes growing on soft agar plates with gradually increasing antibiotic concentrations were able to rapidly evolve resistance to high levels of antibiotics, while sudden jumps to unsustainably high concentrations dramatically slowed down adaptation [12]. These findings raise the theoretical question of how to predict the rate of emergence of drug resistance in the presence of spatial gradients.

A number of recent theoretical studies have investigated how gradients speed up the evolution of drug resistance [26–28]. Each study made critical assumptions about the nature of the gradients: Greulich et al. [27] considered a population adapting to a smooth gradient, which gradually lowers the growth rate of susceptible individuals. Hermsen et al. [26] studied resistance evolution in a series of sharp step-like increases in concentration, where a novel resistance mutations was necessary for survival in the next step (the "staircase" model); Hermsen [28] later proposed a generalization of the staircase model to continuous gradients. These previous studies focused on the speed of adaptation, i.e., how quickly the population evolves to tolerate high concentrations of antibiotics. In the context of the emergence of drug resistance, this observable alone ignores a crucial reality of antibiotic treatment: efficient drug treatment first and foremost aims to kill as many bacteria as possible, while limiting the rise of resistance mutation. How this apparent trade-off can be optimized to prevent the evolution of drug resistance has so far been unexplored. Moreover, many realistic growth scenarios of bacterial populations may exhibit a directed flow that drives them up or down the gradient. Examples include the gut, arteries, and urethra in the human body [29–32], but also flows in aquatic environments, like ocean and river currents [33], or flow in pipes and catheters [34]. The effect of convection on the evolution of drug resistance remains unknown.

Here, we present simulations, rationalized by a comprehensive analytical framework, of populations evolving resistance in a variety of spatial antibiotic concentration

gradients and under the influence of convection. We measure the establishment probability of resistant mutants arising in a region occupied by susceptible wild type, and the drug-induced death rate of the wild type, and show how bacterial diffusion, antibiotic gradient steepness, and convection interact to affect the treatment efficiency. We find that shallow gradients and convection into the antibiotic promote wild-type death, at the cost of increasing the establishment probability of resistance mutations. Conversely, populations in steep gradients and subject to convection away from the antibiotics are less susceptible to drug-induced wild-type death but also produce fewer resistance mutants. The treatment efficiency, which quantifies the inherent trade-off between adaptation and death, is strongly modulated by gradient steepness and convection. Treatment efficiency is found to strongly depend on convection away from the antibiotic, which increases it in shallow gradients and decreases it in steep gradients.

2. Methods

Individual-based simulation

We perform individual-based, stepping stone simulations where both wild-type and mutants are modeled explicitly. The population is divided into demes with carrying capacity K on a one-dimensional lattice. Wild-type and mutants replicate at a rate a_0 and migrate at rate D independently on their position. Wild-type in deme i die at a rate $b(x_i) = \frac{1}{2}[1 + \tanh(mx_i)]$. Since we assume throughout that the antibiotic leaves the mutants unaffected, mutants do not die in our simulations. Analogously to a Gillespie algorithm, in each simulation step, a birth, death or migration event is performed according to its relative rate [35, 36], as follows.

- **Birth.** Birth events occur at a total rate equal to $a_0 \sum_i c(x_i)$, where $c(x_i)$ is the total number of individuals in deme i . For each birth event, a source individual is selected at random and replicated into a random target site between 1 and K within the same deme. Because the target site can either already be filled with an individual or be empty, this move effectively translates into logistic growth within the deme.
- **Death.** In our model, only the wild type can die, thus deaths have a total rate corresponding to $\sum_i b(x_i)c_{\text{wt}}(x_i)$, where $c_{\text{wt}}(x_i)$ represents the number of wild type individuals in deme i . To perform a death event, first, a deme i is picked proportionally to its relative death rate $b(x)c_{\text{wt}}(x_i)$, and then, a random wild type within the same deme selected to be removed.
- **Migration.** Migrations are performed at a rate $D \sum_i c(x_i)$ by picking a random individual and swapping it with a randomly selected target site from one of the two neighboring demes. As in the case of birth events, the target site can either correspond to an individual, or to an empty site.
- **Time step.** Time is tracked by sampling a time interval δt from an exponential distribution with rate $\sum_i [(a_0 + D)c(x_i) + b(x_i)c_{\text{wt}}(x_i)]$, as in a standard Gillespie

algorithm. The total elapsed time is the sum of the sampled time intervals.

- **Convection.** Convection (with convection speed v) is implemented by shifting the simulation box by one deme towards or away from the wild type population, depending on whether convection is negative or positive, respectively. The shift is performed when the time since the last shift is greater than $1/|v|$.

For each simulation, we first allow the wild type to reach the steady-state profile $c(x)$. We then introduce one mutant element at position x and run the simulation until either all mutants go extinct, or mutants reach the last deme in the simulation box. No further mutations are allowed in the course of the simulations. The probability of fixation $u(x)$ is then computed as the proportion of the simulations in which a mutant introduced at x reached fixation.

Numerics

All numerical results were obtained by evaluating the differential equations using Mathematica's built-in *NDSolve* routine with the backwards differentiation (BDF) method, with a maximum step size of 1 and a domain size of 1000. Initial conditions were chosen according to the analytical approximations to the steady-state profiles given in the text. This is only done to speed up computation and increase numerical stability; starting with different initial conditions leads the same final solution. To obtain steady-state profiles, we solve the full time-dependent problems until the solution no longer changes for longer evaluation times.

To compute the establishment probability $u(x)$ in realistic wild-type population profiles $c(x)$, we first computed the steady-state population density and then used the final profile to compute the (constant in time) local death rate for the mutants $b(x) = 1 - c(x)$. The resulting numerical solutions were integrated numerically using Mathematica's built-in *NIntegrate* routine to obtain the total death rate B and the establishment score R .

3. Simulation results

We simulate a population of wild-type individuals on a lattice of L demes, each of size K , in a one-dimensional antibiotic gradient (see the sketch in Fig. 1 and *Methods*). Each individual can migrate into a neighboring deme, replicate, and die. The antibiotic gradient sets the death rate of the wild type, giving rise to an effective growth rate

$$s(x) = \frac{1}{2} [1 - \tanh(mx)]. \quad (1)$$

In the absence of antibiotics, population growth is only limited by a carrying capacity K .

Following the equilibration to the steady-state profile of the wild type, a resistant mutant is inserted into the population at position x . The resistant mutant has the same birth rate as the wild type, but it does not suffer from an increased death rate due to

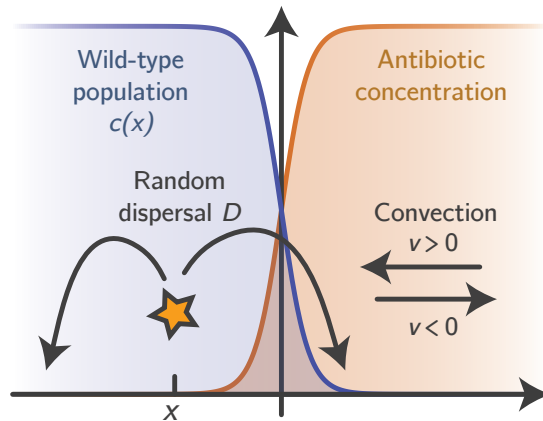


Figure 1. Sketch of our modeling setup. We assume that, initially, a purely wild-type population has reached a steady-state density profile (blue) in the presence of a steady-state antibiotic concentration gradient (orange). Resistance mutations occur spontaneously in randomly drawn individuals and disperse, proliferate and die until extinction or ultimate fixation. Convection can either drive the population towards the antibiotic ($v < 0$) or away from it ($v > 0$). Our goal is to analyze the fixation probability of resistance mutation for a given the rate of wild-type killing.

the antibiotics. We follow the mutant clone until it either goes extinct or reaches the far end of the simulation box, in which case we consider the mutant *established*.

In treating a bacterial infection, the optimal antibiotic strategy would eliminate as many bacteria as possible, while limiting the emergence of resistance. To quantify the treatment efficacy, we first obtain an average wild-type population profile $c(x)$ from independent simulation runs and thus compute the number B of drug-induced wild-type deaths per generation,

$$\text{total death rate } B = \sum_{i=0}^L c(x_i)b(x_i), \quad (2)$$

where $b(x_i)$ is the death rate per generation due to antibiotics in deme x_i . For simplicity, we call B the total death rate.

To quantify the emergence of resistance, we measure the local mutant establishment probability $u(x)$, i.e., the probability that a mutation that arose at position x establishes. Since the probability that a mutation occurs in the first place is proportional to the wild-type population density $c(x)$, it follows that successful mutants can only arise where both the wild-type population density and the establishment probability are high (see Fig. 3). A measure for how readily new resistant mutants establish is thus given by the product of wild-type population density and the establishment probability, summed over all demes x_i [37]. We call this measure the establishment score R ,

$$\text{establishment score } R = \sum_{i=0}^L c(x_i)u(x_i). \quad (3)$$

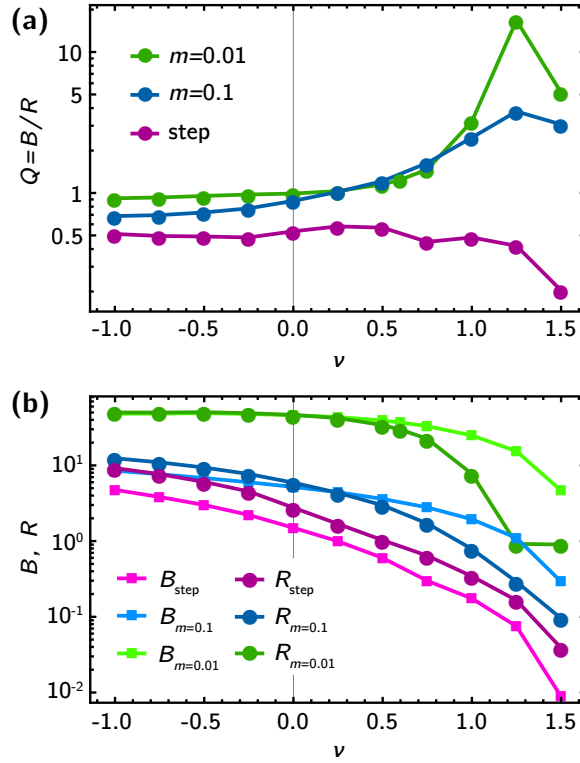


Figure 2. Quantifying the tradeoff between killing of wild-type cells and fixation of resistant mutants. (a) The treatment efficiency Q , defined as the number B of drug-induced deaths per generation divided by the establishment score R (see eq. 4), for different antibiotic concentration profiles (shallow gradient, $m = 0.01$; intermediate gradient, $m = 0.1$; step-like concentration profile). Convection away from the antibiotic (positive v) can increase treatment efficiency by an order of magnitude in shallow gradients. (b) Both B and R are increased (in contrast to their ratio Q) in shallow gradients and for convection into the antibiotic.

The establishment score R is proportional to the rate μR of establishment, the rate at which new resistance mutations arise (at a low mutation rate μ) and establish in the population. Alternatively, the establishment score R can be understood as a measure proportional to the mean establishment probability $\sum c(x_i)u(x_i)/\sum c(x_i)$, i.e., the probability that a mutation arising anywhere in the population establishes.

Finally, we define the efficiency Q of drug treatment via the amount of drug-induced wild-type death B before an adaptive mutation establishes, i.e., by $B/\mu R$. We assume mutation rates to be low such that no clonal interference occurs. Then, we can treat each mutation independently and thus define

$$\text{treatment efficiency } Q = \frac{B}{R}. \quad (4)$$

Fig. 2a shows how the treatment efficiency Q changes across gradient steepness and convection into ($v < 0$) and away from ($v > 0$) the gradient. We find that without convection ($v = 0$), and for convection toward the gradient ($v < 0$), Q is slightly higher for shallow gradients but always bounded between $Q = 0.5$ and $Q = 1$. However,

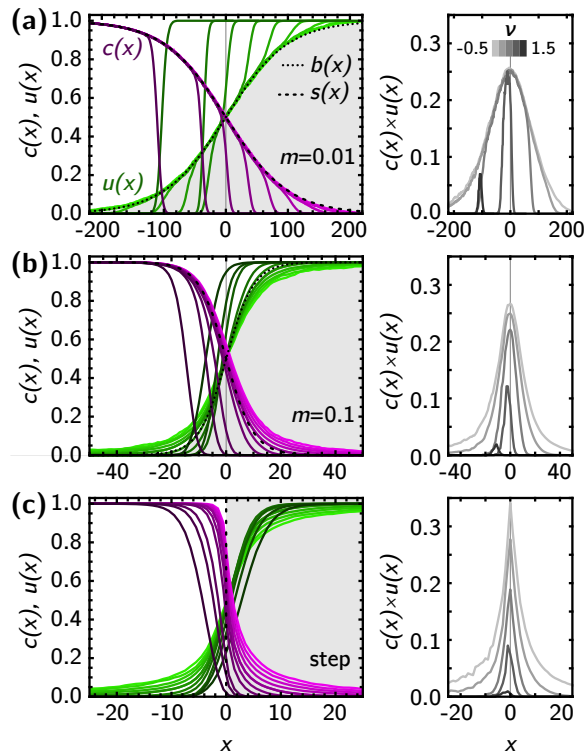


Figure 3. Population density $c(x)$ (magenta) and establishment probability $u(x)$ (green) for three different concentration profiles (gray background; (a) shallow gradient, $m = 0.01$; (b) intermediate gradient $m = 0.1$; (c) step) and different values of $v = -0.5$ to 1.5 (light to dark colors), from stepping stone simulations. Dotted and dashed line are the local wild-type death rate $b(x)$ and the net growth rate $s(x)$. On the right in each panel is the product $c(x)u(x)$, which identifies the region where successful mutants arise.

the trend changes dramatically for positive convection away from the gradient, which boosts treatment efficiency by a factor of 10 for shallow gradients and decreases it for the step-like antibiotic profile.

Considering the establishment score R and the total death rate B separately (Fig. 2b) illustrates the reason behind the qualitative behavior of treatment efficiency. Both R and B show similar tendencies for different gradients and convection speeds: Shallow gradients are characterized by larger values of both R and B than the step-like concentration profile. Negative convection (towards the gradient) increases both R and B by up to a factor of 5, while positive convection leads to their rapid decrease by two orders of magnitude. Remarkably, in shallow gradients the establishment score R is more sensitive than the total death rate B to positive convection. The rapid decrease of R explains the increase in the treatment efficiency $Q = B/R$ for shallow gradients.

A detailed look at the population density $c(x)$ and establishment probability $u(x)$ profiles is necessary to understand the values taken by R and B . These profiles are shown in Fig. 3 for three different gradients (shaded areas). The population density $c(x)$ approximately tracks the net growth rate $s(x)$, while the establishment probability

$u(x)$ is roughly a mirror image of the population density. In the region where the drug concentration is low and the wild-type population is dense, the mutants have no advantage over the wild type, since they compete for the same resources, and are likely to go extinct due to genetic drift. Conversely, in high drug concentration regions, the wild type cannot survive and the mutants can grow freely and establish with high probability.

Convection has a rich variety of effects on both profiles. Convection into the antibiotic (co-flow, $v < 0$) leads to broader profiles of both the wild type population density $c(x)$ and the establishment probability $u(x)$ (Fig. 3), while convection away (counter-flow, $v > 0$) from the antibiotic reduces both the population density and the establishment probability in the antibiotic region. For shallow gradients, we even observe an apparent cut-off in $c(x)$ (and correspondingly in $u(x)$), whose location depends on v . Consequently, co-flow increases total death rate and establishment score, while counter-flow leads to their rapid decrease.

In summary, our simulations show that both the population density profile $c(x)$ as well as the local establishment probability $u(x)$ of resistance mutants are strongly influenced by environmental parameters, in particular, by the steepness of the antibiotic gradient and the strength of convection. As a general rule of thumb, shallow gradients and convection towards increasing drug concentrations increases the establishment score R , while steep gradients and convection away from the drug source decrease it. The total death rate B follows the same trend. However, subtle differences between R and B give rise to a qualitative change in behavior of the treatment efficiency $Q = B/R$, which is increased by positive convection (counter-flow) in shallow gradients and decreased in steep ones. To rationalize our results and identify the critical length scales, we now develop a mathematical model that accommodates these processes.

4. Theory

4.1. Theoretical framework

Consider a population at some density $c(x)$ in an antibiotic concentration field, which gives rise to a death rate $b(x)$ per generation, i.e., the drug-induced death rate is measured relative to the maximum growth rate a_0 . We define the total (drug-induced) death rate B per generation through a continuum version of eq. 2 as

$$B = \int_{-\infty}^{\infty} dx c(x)b(x). \quad (5)$$

Resistance mutations arise at a rate μ , which we assume to be constant and sufficiently low such that adaptation occurs via the sequential acquisition of resistance mutations, i.e., we neglect local clonal interference. Analogously to eq. 3 above, we define the establishment score

$$R = \int_{-\infty}^{\infty} dx c(x)u(x), \quad (6)$$

where $u(x)$ represents the probability that a beneficial mutation born at position x eventually establishes. The population density $c(x)$ can be computed using standard techniques (like deterministic reaction-diffusion equations), and we return to this question later on. The establishment probability $u(x, t)$, i.e., the probability for a mutation to survive until time t , obeys a nonlinear reaction-diffusion equation [37],

$$\partial_t u(x, t) = D\partial_x^2 u + v\partial_x u + s(x)u - a(x)u^2, \quad (7)$$

where $a(x)$ is the local birth rate of the mutants and $s(x) = a(x) - b(x)$ is the net growth rate (see SI section 1). Throughout this paper, we will make the assumption that the birth rate of wild-type and mutant is identical and constant, $a(x) = a_0$, and that the drug-induced death rate of the resistant mutant is zero, while the wild-type drug-induced death rate $b(x)$ ranges from 0 to a_0 , i.e., we assume that the antibiotic only affects the population by increasing the death rate of the wild type. We include diffusion and convection terms to account for the random dispersal and the effects of external flow on the bacteria.

It is important at this point to note that in general the selective gradient $s(x)$ will intimately depend on various environmental factors, including competition with the wild-type population. In later sections, especially when incorporating convection (i.e., $v \neq 0$), we will take this effect into account. For now, we will assume that this function is known for given external conditions in order to gain a better intuition for the system.

4.2. Diffusion without convection

We will first analyze eq. 7 in the case without drift, i.e. $v = 0$, in order to extract the characteristic length scales of the system. We solve the extreme cases of a step-like concentration increase and a very smooth gradient analytically, and then interpolate between the two regimes using numerical solutions to eq. 7.

Step-like gradient

We begin by considering the simplest functional form for a selective gradient – a step:

$$s(x) = a_0\Theta(-x), \quad (8)$$

where $\Theta(x)$ is the Heaviside step function. Such a sharp gradient could emerge, for instance, at the boundary of different tissues or organs with different affinities to store antibiotics [38]. The equation for the fixation probability in this case is given by:

$$0 = \partial_\xi^2 u + \sigma_0\Theta(-\xi)u - u^2 \quad (9)$$

where we have rescaled by the diffusion length scale:

$$\xi = x/L_D, \quad L_D = \sqrt{D/a_0}. \quad (10)$$

In the Appendix, we solve this equation using an analogy from classical mechanics. We have that for $\xi > 0$

$$u(\xi) = \frac{1}{\sqrt{3}} \left(1 + \frac{\xi}{\sqrt{6\sqrt{3}}} \right)^{-2}, \quad (11)$$

implying $u \sim 1/\xi^2$ for large x . For $\xi < 0$, we obtain

$$u(\xi) = \frac{1}{2} \left\{ 3 \tanh^2 \left[\frac{1}{2}(\xi^* - \xi) \right] - 1 \right\}, \quad (12)$$

where $\xi^* = 2 \operatorname{arctanh} \sqrt{\frac{1}{3} + \frac{2}{3\sqrt{3}}}$.

Eq. 11 shows that the fixation probability decays over a characteristic length scale $L_D = \sqrt{D/a_0}$. This length scale can be roughly understood as the typical distance that a mutant individual travels through random dispersal before replicating.

Shallow gradient

Having identified the characteristic length scale over which the establishment probability decays in a step-like concentration profile, we now turn towards more realistic gradients. For simplicity, for the remainder of our calculations, we will model a shallow antibiotic gradient again as the sigmoidal function $\sigma(\xi)$ given in eq. 1, $\sigma(\xi) = \frac{1}{2}[1 - \tanh(m\xi)]$, such that the gradient changes over a characteristic distance $L_m = L_D/m$. Intuitively, if $L_D \gg L_m$, individuals feel sharp, step-like antibiotic transitions within their typical migration distance, and thus, we expect the results of the previous section to remain good approximations. If, conversely, individuals migrate only short distances compared to L_m , i.e., $L_m \gg L_D$, they will sample only a small region of the gradient and will not feel the differences in antibiotics concentration. To make this heuristic idea quantitative, we rescale ξ in eq. 7 by the new length scale L_m to obtain

$$0 = m^2 \partial_\theta^2 u + \sigma(\theta)u - u^2. \quad (13)$$

When $L_m \gg L_D$, i.e., $m \ll 1$, we can neglect the partial derivative in eq. 13, such that

$$u(\xi) = \sigma(\xi) \quad (\text{shallow gradients}). \quad (14)$$

This so-called quasi-static approximation is a straight-forward extrapolation of the well-mixed result and has been used to model establishment in Ref. [27]. For $m \gg 1$, the step-like solution holds, whereas, for $m \approx 1$, no analytical solution is available; in such cases, we solve the equations numerically (see Methods).

To determine which scenario is more relevant in microbial communities, we estimate a typical m . A typical (non-motile) bacterial cell may have a diameter of $1\mu\text{m}$, swimming in a medium of viscosity comparable to that of water (with blood typically only a factor 3 larger than that [39]). Then, its diffusion constant is of order $0.1\text{-}1\mu\text{m}^2/\text{s}$. The length scale $L_D = \sqrt{D/a_0}$ for a typical birth rate of $0.5 - 2\text{hr}^{-1}$ is then between 50 and a few hundred microns. In a microfluidic experiment by Zhang et al. [16], demonstrating facilitation of adaptation through antibiotic gradients, the length scale on which the drug gradient varied was $L_m \approx 200\mu\text{m}$ so that $m \sim 1$ [16].

This estimate is, however, very crude: firstly, the diffusion constant of a bacterium may not be due to thermal fluctuations but due to directed motion that only becomes approximately diffusive on long time scales [40, 41]. In that case, the diffusion constant can be much larger, up to tens or even $100\mu\text{m}^2/\text{s}$. For a bacterium with a division time

of 60 minutes, this leads to a expected typical length $L_D \approx 3\text{mm}$. Indeed, for motile bacteria such as those used in a recent experimental study by Baym et al. [12] with a reported spreading velocity of 40mm/hr, we find $L_D \approx 1 - 10\text{mm}$. Surely, we cannot expect homogeneous antibiotic concentration over such long length scales and indeed step-like transitions in antibiotic concentration were assumed in the study. Therefore, we expect that concentration gradients of significant sharpness should play a key role in both experimental set-ups and practically relevant systems, and hence the quasi-static approximation in eq. 14 should be employed with caution.

4.3. Wild-type population dynamics

As mentioned above, the mutants' net growth rate $s(x)$ generally depends on several environmental factors, including competition with the wild-type population. In addition, both the establishment score R and the total death rate B determined in our simulations depend on the wild-type density profile $c(x)$. To provide analytical expressions for these quantities and the corresponding treatment efficiency Q , we therefore need to accommodate the coupling between wild-type and mutants. In the following, we will employ a simple logistic growth model for the wild-type population and its interaction with the mutant dynamics.

We assume that the wild-type population density $c(x, t)$ is described by the following reaction-diffusion equation:

$$\partial_t c = D \partial_x^2 c + a_{WT}(x) c \left(1 - \frac{c}{K} \right) - b_{WT}(x) c, \quad (15)$$

where $a_{WT}(x)$ is the local wild type birth rate, $b_{WT}(x)$ is the local antibiotic-induced death rate of the wild type. In our model, wild-type growth is limited by a logistic term $(1 - c/K)$, which models a finite amounts of nutrients limiting the population size per deme to the carrying capacity K , while the local death rate $b_{WT}(x)$ acts on each individual independently and is therefore unaffected by the local population density. This distinguishes our model from the Fisher equation used to describe population spreading [42], where also the death rate multiplies the logistic term. Our model instead ensures that the steady-state local population density c_{SS} depends explicitly on the local death rate $b_{WT}(x)$ when the death and birth rate profiles change sufficiently slowly in space,

$$c_{SS}(x) = K \left(1 - \frac{b_{WT}(x)}{a_{WT}(x)} \right). \quad (16)$$

Our model, like the original Fisher equation, ignores the discrete nature of individuals, which has been shown to significantly alter the tip of the population front (see SI section 7 for a detailed discussion). Nevertheless, we expect good agreement between our model and simulations in terms of the treatment efficiency Q , whose value is not significantly affected by the details of the population profile at the tip of the wave.

For the remainder of this text, we will assume, as before, that the total growth rate $a_{WT}(x)$ is a constant, a_0 , and that the presence of the antibiotic modulates selection

by increasing the wild type death rate $b_{WT}(x)$. The logistic growth term makes eq. 15 for the wild type density $c(x)$ mathematically equivalent to eq. 7 for the establishment probability $u(x)$ and hence, all results carry over with minor modifications (eqs. 11, 12, and 14). In particular, the predicted steady-state population density $c(x)$ has a broad tail in the case of a step-like antibiotic profile, and closely follows the mirror image of the antibiotic profile if this is shallow. Note, however, that we are unable to observe the broad tail in simulations because of the discreteness effects associated with the small population size at the front (see SI section 7).

Given an explicit wild-type population profile, it is plausible to assume that the selective pressure felt by the mutants is purely due to competition with the wild type, i.e., $s_{MT}(x) = 1 - c(x)$, such that the local establishment probability of the mutants is coupled to the wild type profile. This should indeed be the case if the antibiotic does not directly alter the birth and death rate of the mutants.

Hence, if $c(x)$ changes sharply, i.e., on length scales shorter than $L_D = \sqrt{D/a_0}$, we expect to see the signatures of a step-like antibiotic profile also in the behavior of $u(x)$. If, on the other hand, $c(x)$ changes slowly in space, then the quasi-static approximation may become applicable. The case of a step-like antibiotic concentration profile $s(x) = s_0\Theta(-x)$ for illustrates both scenarios (see Fig. 4a): for $x < 0$, $c(x)$ approaches 1 exponentially (eq. 12), such that $u(x)$ is well-described by the broad tail in eq. 11. For $x > 0$, instead $c(x)$ decays slowly and the quasi-static approximation can be used such that $u(x) \approx 1 - c(x)$. We compare the simulations with numerical and approximate analytical solutions for $c(x)$ and $u(x)$ in detail in the SI, section 7.

The solutions for $c(x)$ and $u(x)$ can then be used to compute the rate of adaptation R (eq. 6) and total death rate B . Asymptotically, we find,

$$B \approx \sqrt{\frac{D}{a_0}} \times \begin{cases} \sqrt{\frac{\sqrt{12}s_0}{a_0}}, & \text{for } L_D/L_m \ll 1, \\ \frac{s_0}{2a_0m}, & \text{for } L_D/L_m \gg 1, \end{cases} \quad (17)$$

and

$$R \approx \sqrt{\frac{D}{a_0}} \times \begin{cases} 1.8\sqrt{\frac{\sqrt{12}s_0}{a_0}}, & \text{for } L_D/L_m \ll 1, \\ \frac{s_0}{2a_0m}, & \text{for } L_D/L_m \gg 1, \end{cases} \quad (18)$$

which agrees well with the numerical result in the two limiting cases (Fig. 5a). The inverse scaling of the establishment score R with the gradient steepness m is also in agreement with Greulich et al. [27] in relatively steep gradients where the rate of adaptation (which is proportional to the establishment score defined here) is dominated by the time until a mutation arises and establishes. Hermsen [28] also finds that the rate of adaptation increases for shallower (but still relatively steep) gradients in what is identified as the "mutation-limited" regime, where mutations are rare. However, both Hermsen and Greulich consider the establishment of many mutation (potentially simultaneously), giving rise to a second, "dispersion-limited", regime [28] in very shallow gradients, in which the mutational supply is large and the rate of adaptation is dominated by the speed with which established mutations invade

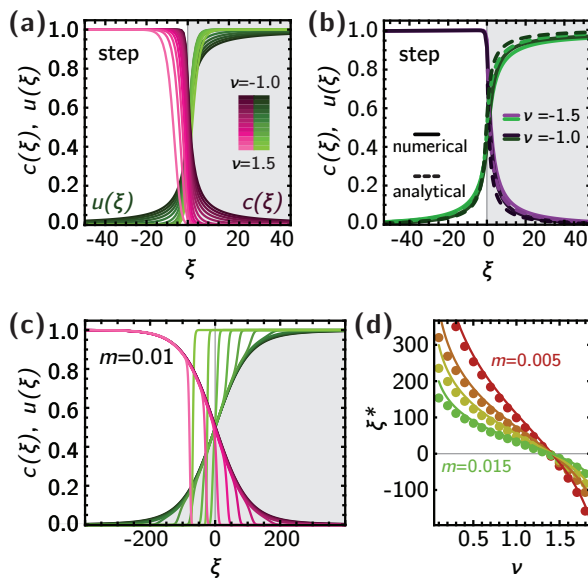


Figure 4. The effect of convection on population density $c(x)$ (magenta) and establishment probability $u(x)$ (green) for a step-like antibiotic concentration (a) and a very broad concentration profile ($m = 0.01$, c), for values of the convection speed ν ranging from -1 to 1.5 in steps of 0.25 (dark to light colors). Curves were obtained by numerically integrating eqs. 19 and 20 (*Methods*). For high negative convection speeds (dark colors), an analytical approximation is valid (b, SI section 5). (d) The cut-off ξ^* of the population density profile in shallow gradients found numerically (dots) agrees well with the theoretical prediction, eq. 22 (solid lines).

previously uninhabitable territory. Since we follow the fate of individual mutations, our model operates in the mutation-limited regime exclusively, and we therefore do not expect agreement between our and their models.

4.4. Convection

So far, we have neglected external flows and only considered random diffusion of individuals in space. In the following, we explore the influence of convection on the population density, the establishment probability, and finally, the treatment efficiency, which, in the absence of convection, is naturally constrained to a relatively small range, see eqs. 17 and 18. When a population is subjected to convection, it will generally move in the direction of the flow, leading to either a depletion or enrichment of both mutant and wild types in the antibiotic region (unless convection is too strong, see SI section 4), depending on whether the flow is directed away (counter-flow) or towards (co-flow) the gradient, respectively. We define the direction of the flow such that a negative convection speed ν points in the positive x -direction, towards the gradient (see Fig. 1). The corresponding equations for $c(\xi, \tau)$ and $u(\xi, \tau)$ are

$$\partial_\tau c = \partial_\xi^2 c + \nu \partial_\xi c + c(\sigma_{WT}(\xi) - c), \quad (19)$$

$$\partial_\tau u = \partial_\xi^2 u - \nu \partial_\xi u + u(1 - c - u), \quad (20)$$

where $\nu = v/\sqrt{Da_0}$. Note the change in sign for the convection term in the equations for $u(\xi)$ and $c(\xi)$ that stems from the reverse time direction in $u(\xi, \tau)$.

Figure 4 shows the effect of convection on both the population density $c(\xi)$ and the establishment probability $u(\xi)$, for a step-like antibiotic profile and a shallow gradient ($m = 0.01$), obtained by first evaluating $c(\xi)$ from eq. 19 and then solving $u(\xi)$ from eq. 20 using the steady-state density profile (see *Methods*).

Consider first the step-like case. There is a strict distinction between positive and negative convection: negative convection (darker colors in Fig. 4a and c) tends to broaden the profiles away from the step and increase both population density and establishment probability near the step. In fact, it can be shown that for our model both profiles decay asymptotically as ν/ξ far from the step in the limit of strong negative convection (Fig. 4b, SI section 5). By contrast, positive convection away from the antibiotic ($\nu > 0$) reduces the wild-type population density in the antibiotic region as well as the establishment probability, giving rise to an exponential decay $c(\xi) \sim e^{-\nu\xi}$ for $\xi > 0$.

The effects of a finite gradient steepness, characterized by the length scale L_m , can be judged by rescaling eq. 19 by L_m , as in eq. 13, i.e.,

$$0 = m^2 \partial_\theta^2 c + m\nu \partial_\theta c + \sigma(\theta)c - c^2. \quad (21)$$

For $\nu < 0$ in shallow gradients, the profiles are barely affected (see Fig. 4c). For $\nu > 0$, on the other hand, convection can alter the profiles strongly: As $m \rightarrow 0$, the solution to eq. 21 first becomes insensitive to the diffusion term and finally also to the convection term, such that the population density profile $c(\xi)$ follows the gradient almost perfectly until it drops steeply to zero at the cut-off position ξ^* (Fig. 4d, see SI section 6), given by

$$\xi^* \propto \frac{\text{arctanh}(1 - \nu^2/2)}{m}. \quad (22)$$

This cut-off position ξ^* captures the behavior of the numerical solution very well (Fig. 4d). The establishment probability $u(\xi)$ mirrors $c(\xi)$ as long as $\xi^* > 0$: for $\xi < 0$, we have $u(\xi) \approx c(-\xi)$, and for $\xi > 0$, we have $u(\xi) \approx 1 - c(\xi)$. For $\xi^* < 0$, $u(\xi)$ increases very sharply from 0 to 1 at the cut-off position, leaving only a very small overlap with $c(\xi)$. Hence, the establishment score R in shallow gradients becomes very small for high positive convection speeds.

Given the scaling of the population density and establishment probability profiles, we can rationalize the behavior of the total death rate B and the establishment score R . As shown in Fig. 5a and b, both B and R increase for negative convection because $c(\xi)$ and $u(\xi)$ maintain broader profiles. In shallow gradients, B and R exhibit a plateau, since $c(\xi)$ and $u(\xi)$ are affected only weakly by negative convection (green). For positive convection, both B and R decrease rapidly by up to 2 order of magnitude for our range of parameters. In shallow gradients, the establishment score R decreases faster than the total death rate B with increasing convection speed because convection affects both $c(\xi)$ and $u(\xi)$ equally, such that their overlap decreases more rapidly than $c(\xi)$ alone

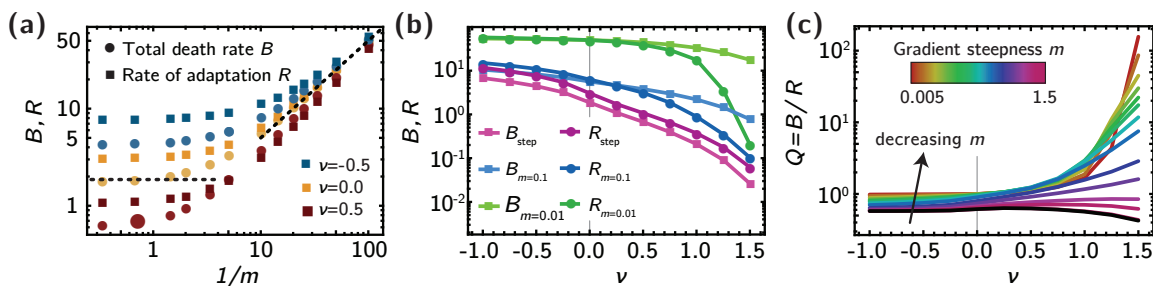


Figure 5. The effect of convection on the establishment score R and the total death rate B in our analytical model. Panel (a) shows R and B as a function of the gradient length scale $L_m = L_D/m$. For $\nu = 0$, the total death rate B approaches the theoretical predictions, eq. 17. Negative/positive convection shifts both B and R up/down, respectively. Plotting B and R as a function of ν in panel (b), we recover the same trend as in stepping stone simulations: negative/positive convection increase/decrease both R and B similarly. (c) The treatment efficiency $Q = B/R$ for a step-like antibiotic profile (black) and gradients of different steepness, from shallow (purple) to steep (red).

(see SI section 6). However, for the steepest gradients, B and R decrease at the same pace until at high convection speeds, the death rate B decreases more quickly than R because of the hard cut-off in $b(\xi)$ (Fig. 5).

The behavior of the treatment efficiency $Q = B/R$ (Fig 5c) follows directly from these considerations. For $\nu < 0$, i.e., for convection into the antibiotic, Q changes only slightly with ν , and only in relatively steep gradients ($m \gtrsim 0.1$). This is in contrast to the case of convection away from the antibiotic: For shallow gradients, i.e., $L_m \gg L_D$, Q is approximately equal to 1 for small positive and all negative convection speeds. For strong positive convection, the establishment score R becomes very small, such that Q increases rapidly (see SI Fig. S2 and SI section 6). As the step-like case is approached, i.e., for $L_m \ll L_D$, the treatment efficiency Q is *reduced* further for large positive ν , where the total death rate B decays more quickly than the establishment score R .

Our numerical findings, supplemented by analytical calculations rationalize all major observations from our simulations. In particular, we find that convection can strongly alter both the total death rate B and the establishment score R , but in a manner that depends on the steepness of the gradient. Although there are subtle differences between the simulated and numerical profiles of c and u (see SI section 7), our simple model reproduces even the complex phenomenology of the treatment efficiency Q , including the shift from an increase in Q in shallow gradients to a decrease in Q in steep ones.

5. Discussion

In order to fight an infection efficiently, an antibiotic must kill as many wild-type bacteria as possible before resistant mutants arise and survive against genetic drift. If a mutant arises in a low-concentration region, it has little advantage over the wild type and likely

goes extinct. By contrast, a mutant arising in a high-concentration background will quickly establish, thus creating a resistant population that can populate regions in the antibiotic gradient inaccessible to the wild type. High population densities in high-concentration regions induce significant wild-type death, as the susceptible wild type cannot survive well in these regions. On the other hand, high population densities in high-concentration regions also maximize the number of resistance mutations that occur in a favorable environment.

We have studied this trade-off between drug-induced wild-type death and adaptation in an antibiotic gradient using simulations and analytical theory. Our simulations reveal that drug-induced death is highest when the wild-type population density is enriched in high-concentration regions, i.e., for convection towards the antibiotic, and shallow gradients. However, since each wild-type individual harbors the potential for a resistance mutation to occur, which would then have a big advantage over the wild type in the region where it occurs, the rate of establishment of resistance mutations has the same general behavior. Similarly, for strong counter-flow, the drug-induced total death rate is decreased because the wild-type population density is low in high-drug regions, which in turn limits the rate of establishment of new resistance mutations. Thus, making ad hoc predictions about the treatment efficiency is difficult. Our detailed analysis of population density $c(x)$ and establishment probability $u(x)$ profiles over a wide range of gradient steepness and convection speeds shows that in shallow gradients, where both $c(x)$ and $u(x)$ are strongly affected by convection away from the antibiotic, treatment can become an order of magnitude more efficient than in no-flow scenarios.

Our simulations are a strongly simplified model of real populations. For instance, we have assumed that mutation establish independently, i.e., we have neglected clonal interference. Our predictions are thus strictly speaking only valid when mutations arise rarely enough that they do not interact. Typically, this condition is quantified by demanding that $\mu N_e \ll 1$, where N_e is the effective population size. In a spatial scenario, however, potentially interfering mutations can only arise in a spatial region where both the population density c and the establishment probability u are large. Thus, our results remain valid as long as $\mu \int c(x)u(x) \ll 1$. For resistance mutations with small target sizes, mutation rates can be very small, typically less than 10^{-6} [43, 44], and thus our approximation may be accurate even for relatively large local populations. In addition, even when mutation rates are not small, we expect convection and spatial gradients to have the same qualitative effects on the establishment of resistance mutations, and thus our results should remain qualitatively correct in this case.

Individuals in our simulation merely occupy "space" in their specific deme; in reality, bacteria have a finite size, and a population front can advance through mere growth, even against strong counter-flow [45]. Conversely, for strong co-flow, individuals may de-adhere and be carried away from the bulk population, thus founding extant colonies that enjoy large growth rates in the absence of competition for resources. Such processes can be studied by generalizing the diffusion term in our model to a long-range

dispersal term as used frequently to model epidemics [46]. Since long-range dispersal can allow individuals far from the population front to escape the bulk population, we expect it to increase the total establishment probability and thus the rate of adaptation relative to short-range dispersal as discussed here.

We have only discussed one-dimensional populations here, but real surface-bound microbial populations typically grow as two-dimensional colonies, with complex spatial patterns. The establishment of beneficial mutations in microbial colonies has recently been discussed [15, 47]. Due to the particular strength of genetic drift at the front of such populations, beneficial mutations first have to reach a threshold size (depending on the strength of the selective advantage) neutrally before they become established. Once the mutant clone reaches the threshold size, the selective advantage of the mutants can deterministically drive them to fixation in the population. During the initial phase, the mutant clone is contained between boundaries with characteristic stochastic properties that are not captured in our one-dimensional model [14]. However, if the threshold size is small, the boundary fluctuations will not have a large impact on the growth of mutant clones. In such cases, we expect our results to apply also to two-dimensional populations.

The emergence of drug resistance remains a topic of significant interest, both from a scientific and a public health point of view. Considerable effort is brought forward to create novel antibiotics [48] and new therapy strategies are developed that attempt to limit the emergence of resistance [49, 50], but more research is needed to understand how resistance evolves in complex spatio-temporal settings like the spatial gradients discussed in this paper. In particular, as we have shown here, convection constitutes an important factor in shaping the adaptation to antibiotics in spatial concentration gradients and should receive more attention from both theorists and experimentalists.

Acknowledgments

Research reported in this publication was supported by the National Institute of General Medical Sciences of the National Institutes of Health under Award Number R01GM115851, by a National Science Foundation Career Award and by a Simons Investigator award from the Simons Foundation (O.H.). The content is solely the responsibility of the authors and does not necessarily represent the official views of the National Institutes of Health. The simulations were run on the Savio computational cluster resource provided by the Berkeley Research Computing program.

Appendix

S1. Derivation of survival probability

Suppose particles branch at rate a and disappear at rate b . Then the probability $u(0; T)$ that a particle or its offspring survive until time T satisfies

$$u(-\epsilon; T) = [1 - \epsilon(a + b)]u(0, T) + \epsilon a [1 - (1 - u(0, T))^2] \quad (\text{S1})$$

The first term on the right-hand side describes the case of neither disappearing nor branching. The second one accounts for the fact that when the initial particle branches then there are two particles, and the probability of survival of at least one lineage is 1 minus the square of both lineages disappearing. Using time-translation invariance $u(-\epsilon; T) = u(T + \epsilon)$, we obtain in the limit $\epsilon \rightarrow 0$

$$\partial_t u(t) = (a - b)u(t) - au^2(t). \quad (\text{S2})$$

To extend this equation for spatial degrees of freedom simply account in eq. S1 for the random jumps to neighboring lattice sites in a small time interval ϵ .

S2. Solving the establishment probability for step-like concentration profile

The (ultimate) establishment probability of a mutation in step-like antibiotic concentration profile given by

$$\sigma(\xi) = \sigma_0 \Theta(-\xi) \quad (\text{S3})$$

satisfies eq. 7 in the main text, repeated here for completeness:

$$0 = \partial_\xi^2 u + \sigma_0 \Theta(-\xi)u - u^2. \quad (\text{S4})$$

To solve this equation, we first treat both sides of the step independently, and then fix integration constants by invoking differentiability at $\xi = 0$.

Antibiotic-free region $\xi > 0$ The fixation probability of mutants in the region $\xi > 0$ (where $\sigma(\xi) = 0$ is determined by the following differential equation:

$$0 = \partial_\xi^2 u - u^2 \quad (\text{S5})$$

with boundary conditions, $u(0) = u_0$ and $u(\infty) = 0$. We exploit a mechanical analogy to solve this equation. We write eq. S5 as

$$\partial_\xi^2 u = -\partial_u V(u) \quad (\text{S6})$$

with a ‘potential energy’ $V(u) = -u^3/3$. We can then determine the solution for $u(\xi)$ as

$$\xi = \int_{u_0}^{u(\xi)} \frac{du'}{\sqrt{-2V(u')}}. \quad (\text{S7})$$

where the ‘total energy’ $E = \frac{1}{2}(\partial_\xi u)^2 + V(u) = 0$ was chosen to satisfy the boundary condition as $\xi \rightarrow \infty$. The solution thus follows as

$$u(\xi) = u_0 \left(1 + \sqrt{u_0} \xi / \sqrt{6}\right)^{-2}, \quad (\text{S8})$$

implying $u \sim 1/\xi^2$ for large ξ .

Antibiotics region $\xi < 0$ In the region $\xi < 0$ the new mutations have a net growth rate $\sigma(\xi) = \sigma_0$. The fixation probability is then given as the solution of

$$\partial_\xi^2 u = -\sigma_0 u + u^2, \quad (\text{S9})$$

Exploiting the same mechanical analogy, we have the integral:

$$\int_{u_0}^u \frac{du}{\sqrt{-\sigma_0 u^2 + 2u^3/3 + \sigma_0^3/3}} = -\xi, \quad (\text{S10})$$

where we have used the condition $u(-\infty) = \sigma_0$ to set the total energy. We obtain

$$u(\xi) = \frac{\sigma_0}{2} \left\{ 3 \tanh^2 \left[\frac{\sqrt{\sigma_0}}{2} (\xi^* - \xi) \right] - 1 \right\}, \quad (\text{S11})$$

where $\xi^* = \frac{2}{\sqrt{\sigma_0}} \operatorname{arctanh} \sqrt{\frac{1}{3} + \frac{2u_0}{3\sigma_0}}$.

At $\xi = 0$, u' is continuous since $u''(0)$ is finite. By imposing continuity on the derivatives from the left and right solutions, we determine $u_0 = \sigma_0/\sqrt{3}$.

S3. Treatment efficiency without convection

To find an approximation for Q in the absence of convection, we can compute B and R independently.

For a shallow gradient where $c(\xi) = s_{\text{WT}}(\xi) = 1 - u(\xi)$, it follows that $B = R$ and hence $Q = 1$. For a steep, B can be obtained directly by simple integration of $c(\xi)$, $B = \sqrt{2} \cdot 3^{1/4}$. To compute R , the integral for $\xi > 0$ is easily performed to yield $R^+ = \frac{2}{3} \sqrt{14/\sqrt{3} - 3}$, but for $\xi < 0$, the full solution for $c(\xi)$ cannot be easily integrated. However, $c(\xi < 0)$ is well approximated by $c(\xi) \approx 1 - (1 - \sqrt{3})e^\xi$. Thus, we obtain the result $R^- = B + 2(\sqrt{3} - 3)e^{\sqrt{3}B} \operatorname{Ei}(-\sqrt{3}B)$, where $\operatorname{Ei}(x) = -\int_{-x}^{\infty} e^{-t}/t$ is the exponential integral function. Q then evaluates to

$$Q \approx 0.581, \quad (\text{S12})$$

close to the numerical value of $Q_{\text{num}} \approx 0.612$.

S4. Strong convection

A population growing logistically with an homogeneous rate across demes leads to a Fisher wave with a front velocity given by $v_F = 2\sqrt{Da_0}$ [42]. In the presence of a convection v , far away from the gradient the wild-type population would generate a front advancing at speed $v_F - v$. Hence, intuitively, if convection is too strong, i.e., $|v| > v_F$, the population will not be able to establish a steady-state profile.

To show this formally, we first transform eq. 17 by introducing a new variable $\psi = ue^{\nu\xi/2}$, such that the convection term is replaced by a death term with effective death rate proportional to ν^2 ,

$$\begin{aligned} \partial_\tau \psi(\xi, \tau) &= \partial_\xi^2 \psi - \frac{\nu^2}{4} \psi + \sigma_0 \Theta(-\xi) \psi - \psi^2 e^{-\nu\xi/2}, \\ \psi(\xi, 0) &= e^{\nu\xi/2}. \end{aligned} \quad (\text{S13})$$

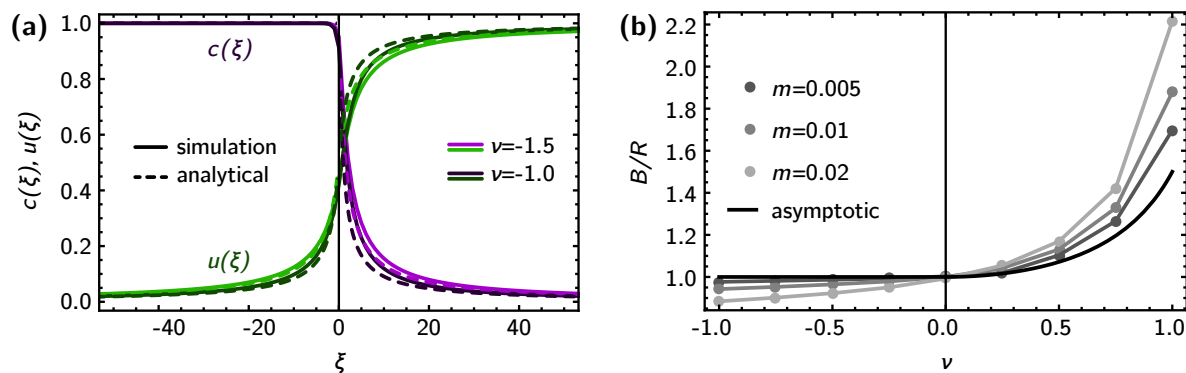


Figure S2. (a) For strong negative convection, the analytical approximations to $c(\xi)$ (eq. S16) and $u(\xi)$ (eq. S17) matches the simulation results well. (b) Treatment efficiency Q for different gradients m , with asymptotic result, eq. S27 (black).

Around $\xi = 0$, the exponential factor is approximately equal to 1 and the nonlinearity ψ^2 can be neglected because $\psi \ll 1$. The resulting linear equation then has solutions that can be written as $\psi = \sum_k a_k(\tau)e^{ik\xi}$. Each mode then satisfies a differential equation

$$\dot{a}_k = -\omega_k a_k, \quad (\text{S14})$$

with $\omega_k = k^2 + \nu^2/4 - \sigma_0$. Thus, the lowest mode $k = 0$ decays to zero as long as $\nu^2/4 - \sigma_0 > 0$, and all higher modes are suppressed by the coupling of modes through the nonlinearity [51]. Therefore, ψ , and hence $c(\xi)$, undergo an extinction transition for $\sigma_0 > 0$ when $\nu^2/4 > \sigma_0$.

S5. Convection in a step-like gradient

Convection into the antibiotics For negative ν , we first solve for $c(\xi)$. For $-2 < \nu \ll 0$, we can neglect diffusion and find the equilibrium population density by solving

$$0 = \nu \partial_\xi c + \Theta(-\xi)c - c^2. \quad (\text{S15})$$

The solution for $\xi > 0$ is

$$c(\xi) = \frac{1}{1 + \xi/|\nu|}. \quad (\text{S16})$$

We thus uncover another characteristic length scale $L_\nu = X\nu = \nu/a_0$, which quantifies the strength of convection relative to diffusion: if $L_\nu \gg L_D$, convection dominates over diffusion, and vice-versa.

Far away from the antibiotics, c will always eventually reach the carrying capacity. Hence, $c(\xi \rightarrow -\infty) \rightarrow 1$, which is a fixed point of eq. S15 for $x < 0$. It follows that $c(\xi < 0) \equiv 1$.

Plugging eq. S16 into the equation for the establishment probability $u(\xi)$, eq. 18 in the main text, we find analytical solutions in two cases: for small but finite negative ν , the convection term and the diffusion term can both be neglected and we recover the

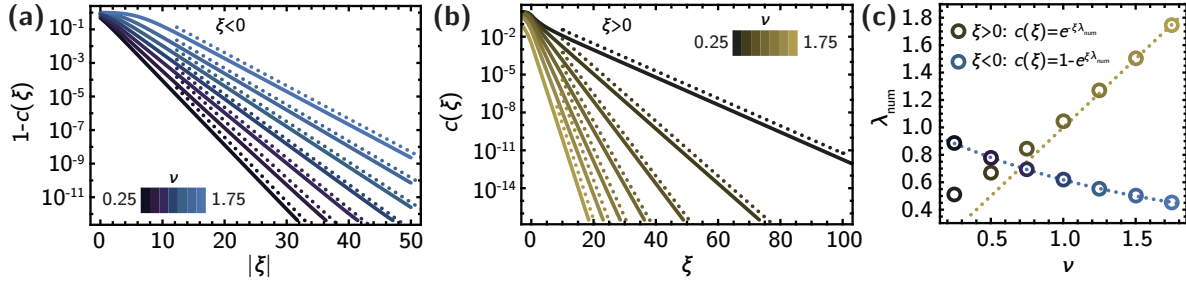


Figure S3. Population density profile for a step-like antibiotic concentration gradient and positive convection $\nu > 0$. Both in the region of high antibiotic concentration ($\xi > 0$) and no antibiotic concentration ($\xi < 0$), the population density approaches its asymptotic value exponentially ((a) and (b), analytical results as dotted lines). Fitting the numerical curves with the analytical expressions, eqs. S22 and S24, we obtain the apparent exponential prefactors λ_{num} , which match well with the expressions for λ_{\pm} given in the text.

quasi-static result $u(\xi) = 1 - c(\xi)$. For strong negative convection, $-2 < \nu \ll 0$, we can neglect only the diffusion term and integrate directly. The result is

$$\begin{aligned} u(\xi) &= \frac{1}{2 - \xi/|\nu|}, & x < 0, \\ u(\xi) &= 1 - \frac{1}{2 + \xi/|\nu|}, & x > 0. \end{aligned} \quad (\text{S17})$$

Since $c(\xi < 0) = 1$, it is easy to see that this approximation does not yield a finite establishment score for infinite domains since mutants arising far away from the antibiotics region still have a relatively high chance of establishing. In practice, the establishment score is always finite because for finite ν , the decay is slightly faster than $1/\xi$. Assuming a finite domain (or a cut-off, e.g., because of a finite carrying capacity) ranging from some $-\xi_0$ to ξ_0 , we can estimate both the establishment score R and the total death rate B , and thus the treatment efficiency $Q = B/R$, as

$$R = \nu \log[1 + \xi_0/\nu] \quad (\text{S18})$$

$$B = 2\nu \log[1 + \xi_0/2\nu] \quad (\text{S19})$$

$$Q = \frac{\log[1 + \xi_0/\nu]}{2 \log[1 + \xi_0/2\nu]} \gtrsim \frac{1}{2} \quad (\text{S20})$$

where we have assumed $\xi_0/\nu \gg 1$ in the last step. In our numerical evaluations, $\xi_0 = 500$ and $\nu < 2$, such that we have $Q \approx 0.57$.

Convection away from antibiotics Positive convection ($\nu > 0$) away from the antibiotic limits diffusion of the wildtype into the antibiotics, thus leading to a reduced wildtype population density in the region of antibiotics. For strong convection and a step-like drug profile, the population density decays exponentially over the characteristic distance X/ν . This follows by considering the steady-state equation for $c(\xi > 0)$,

$$0 = \partial_{\xi}^2 c + \nu \partial_{\xi} c - c^2. \quad (\text{S21})$$

For $\xi > 0$, $c(\xi)^2$ is positive while $c'(\xi)$ is negative; because these two terms cannot add up to zero, we cannot neglect the diffusive term. However, since we expect $c(\xi)$ to be small, we can instead neglect $c(\xi)^2$ to obtain the equation $0 = c'' + \nu c'$, such that

$$c(\xi > 0) \propto e^{-\lambda_+ \xi}, \quad (\text{S22})$$

where $\lambda_+ = \nu$, which approximates the numerical solution well (Fig. S3).

For $\xi < 0$, the corresponding equation reads

$$0 = \partial_\xi^2 c + \nu \partial_\xi c + c - c^2, \quad (\text{S23})$$

which does not have a simple analytical solution. However, we can find by inspection that $c(\xi)$ approximately behaves as

$$1 - c(\xi < 0) \propto e^{-\lambda_- |\xi|}, \quad (\text{S24})$$

where λ_- is parametrized well by $\lambda_- \approx 2/(\nu + \sqrt{\nu^2 + 4})$ (see Fig. S3).

S6. Shallow gradients with convection

For $\nu > 0$ and $L_m \gg L_v$, we can transform eq. 18 by defining $\psi = ce^{-\nu\xi/2}$ to obtain

$$\partial_\tau \psi(\xi, \tau) = \partial_\xi^2 \psi + \left(\sigma(\xi) - \frac{\nu^2}{4} \right) \psi - \psi^2 e^{-\nu\xi/2}. \quad (\text{S25})$$

Convection only has a relatively small effect on $c(\xi)$ and $u(\xi)$, and only in the region of strong antibiotics (where $\sigma(\xi) \ll 1$), as long as $\sigma(\xi) > \nu^2/4$. For large enough ξ this will no longer be satisfied. When $\sigma(\xi) \sim \nu^2/4$, the convection term leads to a cut-off. Assuming the cut-off is faster than exponential, we can neglect the non-linearity near the cut-off and thus find a transition to negative growth rate $\partial_\tau \psi(\xi, \tau)$ for $\sigma(\xi^*) = \nu^2/4$. Solving for ξ^* , we obtain the approximate cut-off position

$$\xi^* = m^{-1} \operatorname{arctanh}(1 - \nu^2/2). \quad (\text{S26})$$

Note that $\xi^* = 0$ for $\nu = \sqrt{2}$. For $\nu < \sqrt{2}$, we can estimate R and B analytically by approximating $c(\xi) \approx \sigma(\xi)\Theta(\xi - \xi^*)$ and similarly for $u(\xi)$. This leads to

$$Q = \frac{1}{2} + \frac{1}{2 - \nu^2}. \quad (\text{S27})$$

For $\nu < \nu^*$, this agrees well with the numerical result for shallow gradients ($m \ll 1$), as shown in Fig. S2. When $\xi^* < 0$, i.e., when $\nu > \sqrt{2}$, $c(\xi)$ and $u(\xi)$ retain a small overlap, as shown in Fig. 4b in the main text. Hence, the treatment efficiency Q does not diverge at ν^* .

S7. Comparing simulations and numerics

Our model for the dynamics of the population density, like the original Fisher equation, ignores the discrete nature of individuals. This has been shown to have important consequences, particularly at the tip of the population front, where the number of individuals per deme is small. A heuristic way to implement the discreteness of individuals consists in introducing a cut-off in the growth rate when the local population

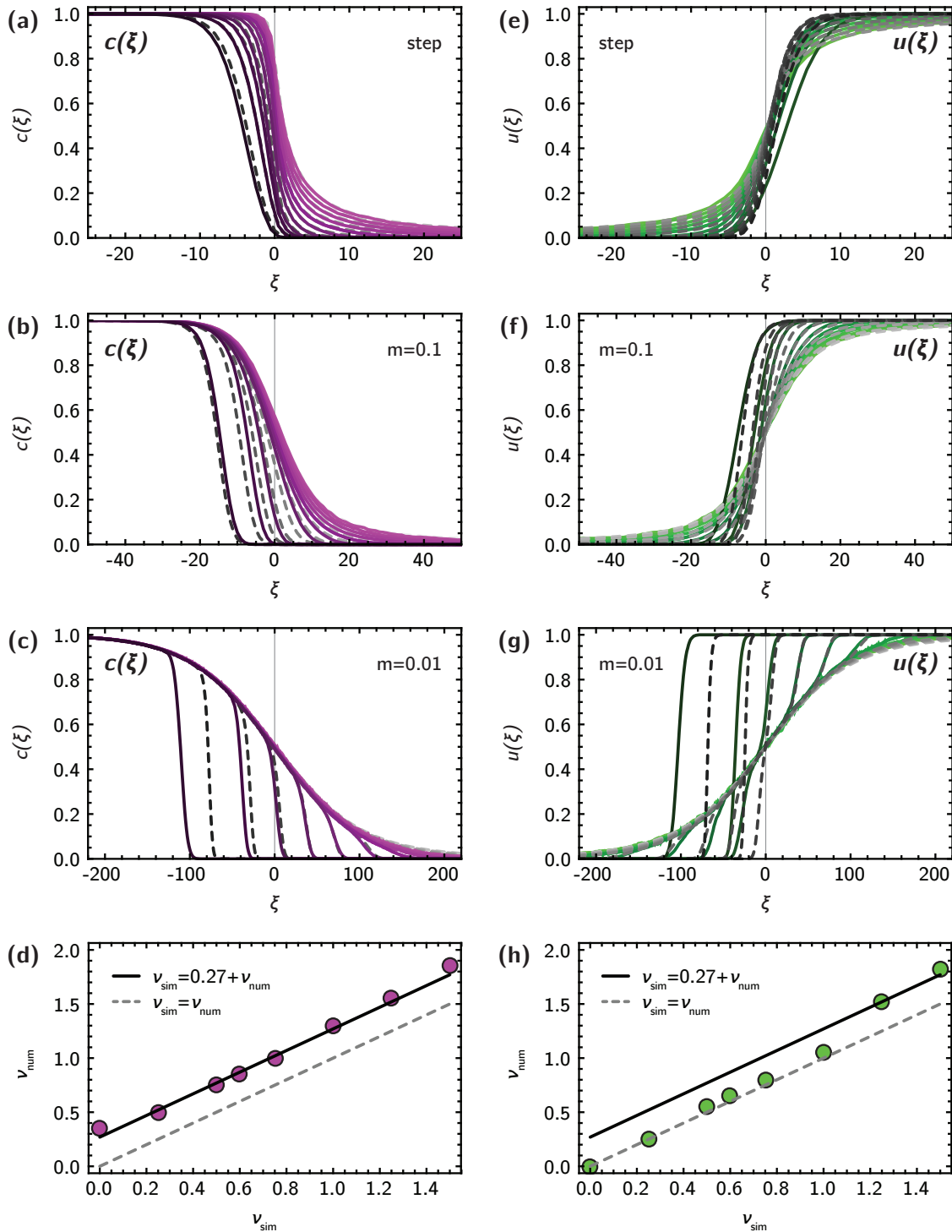


Figure S4. Comparison between simulated (solid lines) and numerically evaluated (dashed gray) profiles of population density $c(\xi)$ (left column, magenta) and establishment probability $u(\xi)$ (right column, green), for three different antibiotic gradients (step-like, (a) and (e); intermediate gradient $m = 0.1$, (b) and (f); shallow gradient $m = 0.01$, (c) and (g)). Deviations between simulations and our numerical model can be traced back to a difference in effective convection speed: the population density feels a slightly higher effective convection ν_{num} (d), while the establishment probability profile reflects the actual convection speed in the simulation ν_{sim} (h) until the deviations in $c(\xi)$ become too large at high ν_{sim} .

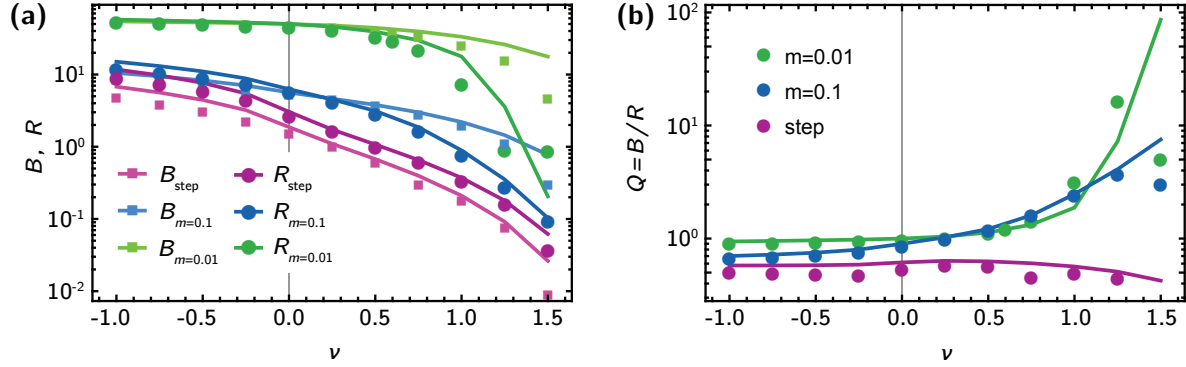


Figure S5. (a) Good agreement between simulated (dots) and numerically evaluated (lines) total birth rate B and establishment score R . Deviations appear mainly at high positive convection speeds $\nu \gg 0$ in shallow gradients, where the wave front is characterized by strong fluctuations (see Fig. S4 and SI Section 7). (b) Our theory reproduces the observed trends of the treatment efficiency Q except for the highest positive convection speeds.

size becomes too small [52]. Such a cut-off alters the front profile, and the resulting correction to the expansion velocity decays only slowly with the carrying capacity K ,

$$v_F^* = v_F \left(1 - \frac{\pi^2}{2 \ln^2 K} \right). \quad (\text{S28})$$

In our simulations, we use $K = 100$, which should lead to a correction to the velocity by almost 25%. Quantitative comparison between numerics and simulations reveals such correction. In shallow gradients with positive convection, where the population density and establishment probability profiles are effectively cut off at a characteristic position ξ^* (see eq. S26), we compute the effective convection speed by comparing the cut-offs in simulated profiles with the numerical curves. The results are shown in Fig. S4(d) and (h): the population density obtained from simulations at convection speed ν_{sim} has cut-offs positions corresponding to a numerical convection speed ν_{num} that is shifted up by a constant. For instance, even at $\nu_{\text{sim}} = 0$, we observe a cut-off consistent with a convection speed $\nu_{\text{num}} = 0.27$. The same shift is not visible in the apparent convection speeds obtained from the establishment profiles; in this case, $\nu_{\text{sim}} = \nu_{\text{num}}$, except for very high velocities, where $u(\xi)$ is entirely determined by the population density profile $c(\xi)$ (which deviates from the analytical prediction, see Fig. S4c).

Despite these subtle deviations between our model and simulations, we expect good agreement as long as the population density is not too small; Since the establishment probability $u(x)$ is typically low where the wildtype density $c(x)$ is high and vice-versa, and the establishment score R depends only on the product of $c(x)$ and $u(x)$, regions of small population density should not significantly impact the integral in most cases. Fig. S5 shows that there is indeed good agreement between the establishment score R , the total death rate B and the treatment efficiency Q obtained from simulations and from numerical evaluation of our model.

References

- [1] Neu H C 1992 *Science* **257** 1064–1073
- [2] Spellberg B, Guidos R, Gilbert D, Bradley J, Boucher H W, Scheld W M, Bartlett J G, Edwards J and the Infectious Diseases Society of America 2008 *Clinical Infectious Diseases* **46** 155–164
- [3] Davies J and Davies D 2010 *Microbiology and Molecular Biology Reviews* **74** 417–433
- [4] Levy S B and Marshall B 2004 *Nature Medicine* **10** S122–S129
- [5] Lambert G, Estévez-salmeron L, Oh S, Liao D, Emerson B M, Tlsty T D and Austin R H 2011 *Nature reviews. Cancer* **11** 375–382
- [6] Raguz S and Yagüe E 2008 *British journal of cancer* **99** 387–391
- [7] Blair J M, Webber M A, Baylay A J, Ogbolu D O and Piddock L J 2015 *Nature Reviews Microbiology* **13** 42–51
- [8] Toprak E, Veres A, Michel J B, Chait R, Hartl D L and Kishony R 2012 *Nature genetics* **44** 101–5
- [9] Allen R and Waclaw B 2016 *Physical biology* **13** 045001
- [10] Ramsayer J, Kaltz O and Hochberg M E 2013 *Evolutionary Applications* **6** 608–616
- [11] MacLean R C, Hall A R, Perron G G and Buckling A 2010 *Nature Reviews Genetics* **11** 405–414
- [12] Baym M, Lieberman T D, Kelsic E D, Chait R, Gross R, Yelin I and Kishony R 2016 *Science* **353** 1147 – 1151
- [13] Ling S, Hu Z, Yang Z, Yang F, Li Y, Chen Q, Gong Q, Wu D, Li W, Tian X, Hao C, Hungate E A, Daniel V T, Hudson R R, Li W h, Lu X, Ling S, Hu Z, Yang Z, Yang F, Li Y, Lin P, Chen K, Dong L and Cao L 2016 *Proceedings of the National Academy of Sciences* **113** E663–E663
- [14] Fusco D, Gralka M, Anderson A, Kayser J and Hallatschek O 2016 *Nature Communications* **7** 1–9
- [15] Gralka M, Stiewe F, Farrell F, Möbius W, Waclaw B and Hallatschek O 2016 *Ecology letters* **19** 889–898
- [16] Zhang Q, Lambert G, Liao D, Kim H, Robin K, Tung C k, Pourmand N and Austin R H 2011 *Science* **333** 1764–1767
- [17] Bell G and Gonzalez A 2011 *Science (New York, N.Y.)* **332** 1327–30
- [18] Bell G and Gonzalez A 2009 *Ecology letters* **12** 942–8
- [19] Martinez J L 2009 *Proceedings of the Royal Society B: Biological Sciences* **276** 2521–2530
- [20] Andersson D I and Hughes D 2014 *Nature reviews. Microbiology* **12** 465–78
- [21] Stewart P S and William Costerton J 2001 *The Lancet* **358** 135–138

- [22] Elliott A M, Beming S E, Iseman M D and Peloquin C A 1995 *Tubercle and Lung Disease* **76** 463–467
- [23] Meulemans A, Paycha F, Hannoun P and Vulpillat M 1989 *Antimicrobial agents and chemotherapy* **33** 1286–1290
- [24] Minchinton A I and Tannock I F 2006 *Nature Reviews Cancer* **6** 583–592
- [25] Kepler T B and Perelson A S 1998 *Proceedings of the National Academy of Sciences* **95** 11514–11519
- [26] Hermsen R, Deris J B and Hwa T 2012 *Proceedings of the National Academy of Sciences* **109** 10775–10780
- [27] Greulich P, Waclaw B and Allen R J 2012 *Physical Review Letters* **109** 088101
- [28] Hermsen R 2016 *Physical Biology* **13** 065003
- [29] Passerini L, Lam K, Costerton J W and King E G 1992 *Critical Care Medicine* **20** 665–673
- [30] Hall-Stoodley L, William Costerton J and Stoodley P 2004 *Nature Reviews Microbiology* **2** 95–108
- [31] Persat A, Nadell C D, Kim M K, Ingremeau F, Siryaporn A, Drescher K, Wingreen N S, Bassler B L, Gitai Z and Stone H A 2015 *Cell* **161** 988–997
- [32] Cremer J, Segota I, Yang C y, Arnoldini M, Sauls J T, Zhang Z, Gutierrez E, Groisman A and Hwa T 2016 *Proceedings of the National Academy of Sciences* 201601306
- [33] Battin T J, Sloan W T, Kjelleberg S, Daims H, Head I M, Curtis T P and Eberl L 2007 *Nature reviews. Microbiology* **5** 76–81
- [34] Stickler D J 2008 *Nature Clinical Practice Urology* **5** 598–608
- [35] Gillespie D T 1976 *Journal of computational physics* **22** 403–434
- [36] Gillespie D T 1977 *The journal of physical chemistry* **81** 2340–2361
- [37] Lehe R, Hallatschek O and Peliti L 2012 *PLoS Comput Biol* **8** e1002447
- [38] Fu F, Nowak M A and Bonhoeffer S 2015 *PLoS Comput Biol* **11** e1004142
- [39] Rand P W, Lacombe E, Hunt H E and Austin W H 1964 *J. Appl. Physiol.* **19** 117–122
- [40] Wu X L and Libchaber A 2000 *Physical Review Letters* **84** 3017–3020
- [41] Kim M J and Breuer K S 2004 *Physics of Fluids* **16** 78–81
- [42] Fisher R A 1937 *Annals of eugenics* **7** 355–369
- [43] Martinez J L and Baquero F 2000 *Antimicrobial Agents and Chemotherapy* **44** 1771–1777
- [44] Woodford N and Ellington M J 2007 *Clinical Microbiology and Infection* **13** 5–18
- [45] Tesser F, Zeegers J C H, Clercx H J H, Brunsveld L and Toschi F 2016 URL <http://arxiv.org/abs/1608.07959>

- [46] Hallatschek O and Fisher D S 2014 *Proceedings of the National Academy of Sciences* **111** E4911–E4919
- [47] Lavrentovich M O, Korolev K S and Nelson D R 2013 *Physical Review E* **87** 012103
- [48] Seiple I B, Zhang Z, Jakubec P, Langlois-Mercier A, Wright P M, Hog D T, Yabu K, Allu S R, Fukuzaki T, Carlsen P N *et al.* 2016 *Nature* **533** 338–345
- [49] Enriquez-Navas P M, Kam Y, Das T, Hassan S, Silva A, Foroutan P, Ruiz E, Martinez G, Minton S, Gillies R J *et al.* 2016 *Science translational medicine* **8** 327ra24–327ra24
- [50] Paterson I K, Hoyle A, Ochoa G, Baker-Austin C and Taylor N G H 2016 *Scientific Reports* **6** 37853
- [51] Dahmen K A, Nelson D R and Shnerb N M 2000 *Journal of mathematical biology* **41** 1–23
- [52] Brunet E and Derrida B 1997 *Physical Review E* **56** 2597–2604